Neoplasia • Vol. 8, No. 4, April 2006, pp. 259–267 259

www.neoplasia.com

The Functional Diffusion Map: An Imaging Biomarker for the Early Prediction of Cancer Treatment Outcome[1]

Bradford A. Moffat, Thomas L. Chenevert*,[2], Charles R. Meyer*, Paul E. Mckeever[†], Daniel E. Hall*, Benjamin A. Hoff*, Timothy D. Johnson[‡], Alnawaz Rehemtulla[§,2] and Brian D. Ross*,[2]*

Center for Molecular Imaging, Departments of *Radiology, [†]Pathology, [‡]Biostatistics, and [§]Radiation Oncology, University of Michigan School of Medicine, Ann Arbor, MI, USA

Abstract

Functional diffusion map (fDM) has been recently reported as an early and quantitative biomarker of clinical brain tumor treatment outcome. This MRI approach spatially maps and quantifies treatment-induced changes in tumor water diffusion values resulting from alterations in cell density/cell membrane function and microenvironment. This current study was designed to evaluate the capability of fDM for preclinical evaluation of dose escalation studies and to determine if these changes were correlated with outcome measures (cell kill and overall survival). Serial T_2-weighted and diffusion MRI were carried out on rodents with orthotopically implanted 9L brain tumors receiving three doses of 1,3-bis(2-chloroethyl)-1-nitrosourea (6.65, 13.3, and 26.6 mg/kg, i.p.). All images were coregistered to baseline T_2-weighted images for fDM analysis. Analysis of tumor fDM data on day 4 posttreatment detected dose-dependent changes in tumor diffusion values, which were also found to be spatially dependent. Histologic analysis of treated tumors confirmed spatial changes in cellularity as observed by fDM. Early changes in tumor diffusion values were found to be highly correlative with drug dose and independent biologic outcome measures (cell kill and survival). Therefore, the fDM imaging biomarker for early prediction of treatment efficacy can be used in the drug development process.

Neoplasia (2006) **8,** 259–267

Keywords: Functional diffusion map (fDM), MRI, glioma, therapeutic efficacy, imaging biomarker.

Introduction

The large number of water molecules contained within tumor tissues provides an important opportunity to quantify their respective random trajectories (i.e., diffusion or Brownian motion) for use as a noninvasive microscopic probe to assess changes in tumor cell membrane integrity following treatment intervention. This can be accomplished based on the use of diffusion magnetic resonance imaging (MRI) pulse sequences, which allows for three-dimensional tumor images where the MR signal is dependent on the mobility of water molecules within the tissue of interest [1]. Water can reside within an intracellular compartment, where it is in a more restricted environment relative to the extracellular compartment; thus, intracellular water has lower apparent water mobility (diffusion value). Changes in the ratio of the extracellular to intracellular compartmental volumes (V_e/V_i) will significantly affect the overall mobility of water within that measured tissue region on the diffusion MR image. Treatment of a tumor with an effective cytotoxic agent will result in an increase in the value of the V_e/V_i ratio due to loss of cell membrane integrity and subsequent loss in overall cellular density. Relative tissue contrast on diffusion tumor maps is directly related to diffusion values for each voxel in the image; therefore, the overall net effect of a successful treatment would be an increase in the fractional volume of the interstitial space, resulting in an increase in water diffusion.

The application of diffusion MRI for the detection of early tumor treatment response was first reported using a rodent glioma model [2]. Subsequent publications have verified and expanded this initial report using several different tumor models and therapeutic agents [3–27]. Taken together, these studies have shown that diffusion MRI is a sensitive biomarker that is capable of detecting early cellular changes in treated tumors, which precede macroscopic volumetric response. In addition, it was also reported that diffusion MRI is a sensitive technique that allows for the identification of spatially distinct regional responses to therapy within tumor tissues [13,14,16–18,20]. Until recently, animal studies compared the mean apparent diffusion coefficient (ADC) value from the entire tumor mass posttherapy to the baseline (pretreatment) mean ADC value. However, the response of ADC to cytotoxic therapy in the clinical setting was found to be more complex due to heterogeneity observed within human tumors [11]. During the treatment of patients with malignant brain tumors, it was shown that diffusion changes could both increase (loss of intracellular

Abbreviations: MRI, magnetic resonance imaging; T_2, MRI transverse relaxation time; ADC, apparent diffusion coefficient; fDM, functional diffusion map

Address all correspondence to: Brian D. Ross, Department of Radiology, University of Michigan, MSRB III, Room 9303, Ann Arbor, MI 48109-0648. E-mail: bdross@umich.edu

[1]This work was supported, in part, by research grants from the National Institutes of Health/National Cancer Institute (PO1CA85878, R24CA83099, and P50CA093990).

[2]Disclosure: T.L.C., A.R., and B.D.R. have financial interests in the technology presented in this manuscript.

DOI 10.1593/neo.05844

space) and decrease (increase in intracellular space) over time within the same tumor volume, especially for treatments with modest efficacy [11,28]. This complicated response scenario rendered the use of the mean change in overall tumor ADC values less sensitive due to opposite and competing effects. This observation required the development of a new approach that could provide for the separation and quantification of these competing changes. The idea was that the V_e/V_i ratio could either increase or decrease during tumor treatment; thus, both of these events required identification within the diffusion image. To this end, functional diffusion map (fDM) was developed as a statistical approach for segmenting tumors based on a defined threshold of ADC change following therapy [28].

Results from patients with primary malignant brain tumors were analyzed using the fDM approach, which revealed that the volume of fDM response had a strong correlation with the overall clinical response based on the World Health Organization response criteria [28]. A more recent study [29], wherein patients with grade III/IV gliomas were analyzed using fDM, revealed that fDM could be used to stratify patients as responsive or nonresponsive to therapy in as early as 3 weeks into a 6-week to a 7-week fractionated therapy schedule. In this study, patients identified by fDM as nonresponsive had significantly poorer survival and time-to-progression than patients identified as responsive [29]. Thus, fDM has emerged as a predictive biomarker for the early stratification of tumor response before therapy completion. The purpose of this current study was to evaluate fDM as an early, sensitive, and predictive tumor imaging biomarker in the preclinical setting using a rodent glioma model. This study is vitally important as it provides an opportunity to further assess the fDM approach using a well-controlled experimental tumor model.

The sensitivity of fDM was assessed by quantifying diffusion changes in rat 9L tumors treated with different doses of 1,3-bis(2-chloroethyl)-1-nitrosourea (BCNU)—a cytotoxic drug often used clinically for the treatment of malignant gliomas. Three-dimensional fDM maps were computed from MRI data obtained from individual animals pretherapy and posttherapy. Analysis of tumor fDM data as early as 4 days posttreatment was found to detect dose-dependent changes in ADC maps. In addition, these changes were also found to be spatially dependent and were found to correlate with histologic changes in tumor cell density. These early treatment–induced changes in tumor diffusion properties were also found to be highly correlated with drug dose and animal survival, suggesting that fDM is a valid early predictive biomarker for treatment efficacy. The fDM biomarker has potentially broad applications in preclinical drug development and in the individualization of cancer patient management.

Materials and Methods

Intracranial Tumor Implantation

All animal works were carried out in the animal facility of the University of Michigan (Ann Arbor, MI) in accordance with federal, local, and institutional guidelines. Intracerebral brain tumors were implanted in male Fischer 344 rats (Charles River Breeding Laboratories, Wilmington, MA) weighing between 125 and 150 g. Animals were anesthesized by intraperitoneal administration of a ketamine (87 mg/kg)/xylazine (13 mg/kg) mixture. A small skin incision was made over the right hemisphere, and a 1-mm-diameter burr hole was drilled through the skull. A sterile suspension of 1×10^5 9L cells in 5 μl of serum-free medium was introduced through a 27-gauge needle inserted to a depth of 3 mm. Rats were allowed to recover after filling the burr hole with bone wax and suturing the skin closed.

Chemotherapy

Thirty-three animals with 9L tumors were entered into the study. When *in vivo* tumor volumes had reached 20 to 60 μl, animals were divided into four groups. Group 1 received 0.1 ml of drug vehicle (10% ethanol) and was used as a control group ($n = 7$). Groups 2 to 4 received 6.65 mg/kg BCNU ($n = 7$), 13.3 mg/kg BCNU ($n = 11$), and 26.6 mg/kg BCNU ($n = 8$), respectively, diluted in 10% ethanol. All treatments were administered by a single intraperitoneal injection on day 0. T_2-weighted (T_2, MRI transverse relaxation time) and diffusion MRI were performed every other day posttherapy to measure volumetric and cell density changes, respectively. Animal survival data were also obtained for all groups.

Diffusion MRI

Maps of tumor ADC values were acquired every other day up to 14 days posttherapy using a previously described method [11]. Briefly, a trace diffusion–weighted multislice spin echo sequence (with motion compensation and navigator echo) was used to acquire 13 slices with two different diffusion weightings [$b_1 = 100$ sec/mm^2; $b_2 = 1248$ sec/mm^2; image slice thickness = 1 mm; image matrix = 128 $\times$ 128 (0–256); field of view = 30 $\times$ 30 mm; echo time = 60 milliseconds]. During all MRI procedures, the animals were anesthesized with 1.5% isoflurane, and body temperature was maintained at 37°C using a heated water-recirculating pad. The images acquired with b_1 were essentially T_2-weighted images, and these were used to segment the tumor from the normal brain for volumetric analysis using an "in-house" region drawing tool developed in MATLAB (Natick, MA).

Image Registration and fDM

An important part of fDM analysis is the registration of parametric ADC maps acquired posttherapy to baseline ADC maps acquired before treatment. Image registration was performed using an automated linear affine coregistration algorithm (MIAMI Fuse; University of Michigan, Ann Arbor, MI) to maximize mutual information between the two temporally distinct three-dimensional data sets [30]. Following registration and tumor segmentation of voxels within the tumor both at baseline and on day 4, fDM statistics were calculated. Firstly, ADC values of voxels posttherapy were plotted as a function of baseline ADC values. These tumor voxels were then further segmented into three regions based on an upper threshold and a lower threshold of ADC change.

That is, tumor voxels that had increased ADC above the upper threshold were region 1 (V_R, red voxels), voxels that had decreased below the lower threshold were region 2 (V_B, blue voxels), and all other voxels were region 3 (V_G, green voxels). A comparison between treatment groups and the measurement of fDM dose dependence was accomplished to optimize the sensitivity of the thresholds used ($\pm 0.4 \times 10^{-9}$ m^2/sec). Normalized volumes were then calculated for each animal, and group statistics were calculated.

Histopathology

In a separate study consisting of eight animals, two animals per treatment group were imaged pretreatment and again at 6 to 7 days posttherapy. Following the second imaging session, animals were euthanized, and the brains were fixed in 10% paraformaldehyde. After 48 hours, fixed tissues were transferred to 70% ethanol and embedded in paraffin. Formalin-fixed paraffin-embedded specimens were serially sectioned and slide-mounted. Sections were stained with hematoxylin and eosin (H&E) and compared to fDMs. This was accomplished to identify underlying histologic changes associated with observed regional alterations in fDMs.

Tumor Cell Kill Calculations and Statistical Analysis

The quantification of tumor cell kill from serially volumetric imaging data for each animal was accomplished as previously described [31]. In brief, $\log(\text{cell kill}) = \log_{10}[V_{pre}/V_{post}]$, where V represents the tumor volume from MRI. Linear least squares analysis was used to measure the statistical significance of trends in the BCNU dose dependence of fDM volume, animal survival, and log cell kill, and in the correlation of fDM response with survival and cell kill. When two groups were compared, a one-tailed Student's t test was used. Both linear least squares and Student's t test were performed using Microsoft Excel (Microsoft, Redmond, WA). To compare the median survival of all four animal groups, a log rank test was performed using Prism (GraphPad Software, Inc., San Diego, CA).

Results

Objective assignment of threshold-defining fDM regions is required to provide optimal sensitivity for the detection of therapy-induced changes. In this study, the normalized tumor volume of region 1 (V_R) was plotted (Figure 1*a*) as a function of decreasing upper threshold for the four groups of animals investigated. Analysis of these data revealed that upper thresholds of 0.2×10^{-9}, 0.3×10^{-9}, and 0.4×10^{-9} m^2/sec were all able to statistically differentiate between the three treatment groups, and between the treatment groups and the control group. At these thresholds, based on a one-tailed t test, V_R was statistically different ($P < .05$) for all groups, with V_R being greater for the 26.6-mg/kg, 13.3-mg/kg, 6.65-mg/kg, and control groups. In contrast, the same plot for the lower threshold (Figure 1*b*) revealed that there was no statistical difference ($P > .05$) between the normalized volume of region 2 (V_B) for the control and the 6.65-mg/kg groups, the 6.65- and the 13.3-mg/kg groups, or the 13.3- and the 26.6-mg/kg groups. However, the higher V_B values of control animals were found to be statistically significant ($P < .05$) compared to the 13.3- and 26.6-mg/kg animals for thresholds of -0.1×10^{-9} and -0.2×10^{-9} m^2/sec. To minimize the V_R and V_B volumes of the control group while maintaining sensitivity to treatment-induced changes, a threshold of $\pm 0.4 \times 10^{-9}$ m^2/sec was used to identify/segment the three fDM regions for all fDM images, scatter plots, and subsequent statistical comparisons with outcome efficacy measures.

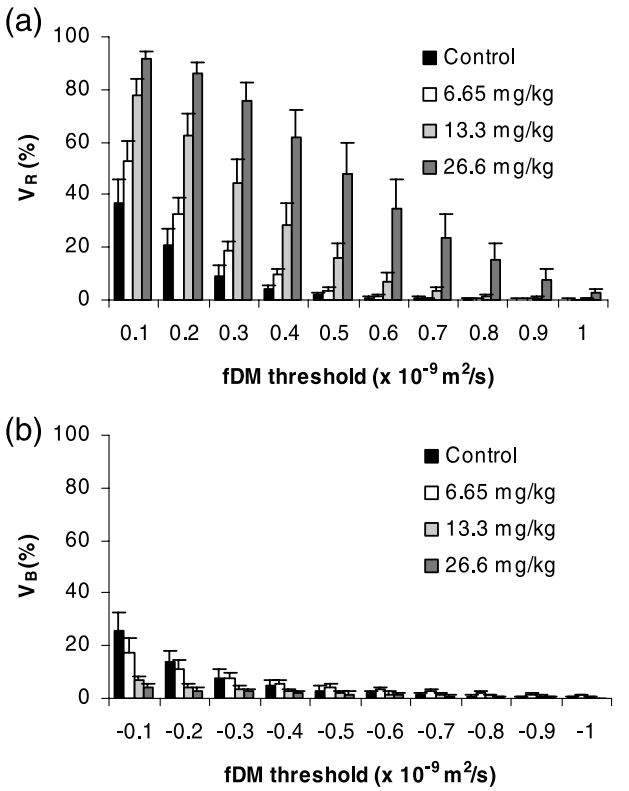

Figure 1. *fDM region volumes as a function of fDM threshold for the different treatment groups. (a) The change in V_R as a function of the upper threshold of ADC change (m^2/sec). (b) The change in V_B as a function of the lower threshold of ADC change (m^2/sec). The bars represent the mean V_R and V_B for each group at a given threshold, and the error bars represent the standard error of the mean.*

Functional diffusion mapping is a spatial mapping technique that segments diffusion MRI voxels within a tumor into three distinct regions of diffusion change. Region 1 consists of voxels wherein the change in ADC values from baseline to posttherapy was greater than an upper threshold. These regions are shown as red pixels on fDM images (Figure 2, *a*, *c*, *e*, and *g*) and as red data points on fDM scatter plots (Figure 2, *b*, *d*, *f*, and *h*). Region 2 represents voxels in which the ADC change was less than a lower threshold and is shown as blue pixels on fDM images and as blue data points on scatter plots (Figure 2). Region 3 comprises voxels for which ADC change was within the two thresholds and is shown as green pixels and data points in Figure 2. These examples of fDM images and scatter plots were taken from a representative animal from each of the groups on day 4 posttreatment. The control tumor example (Figure 2, *a* and *b*)

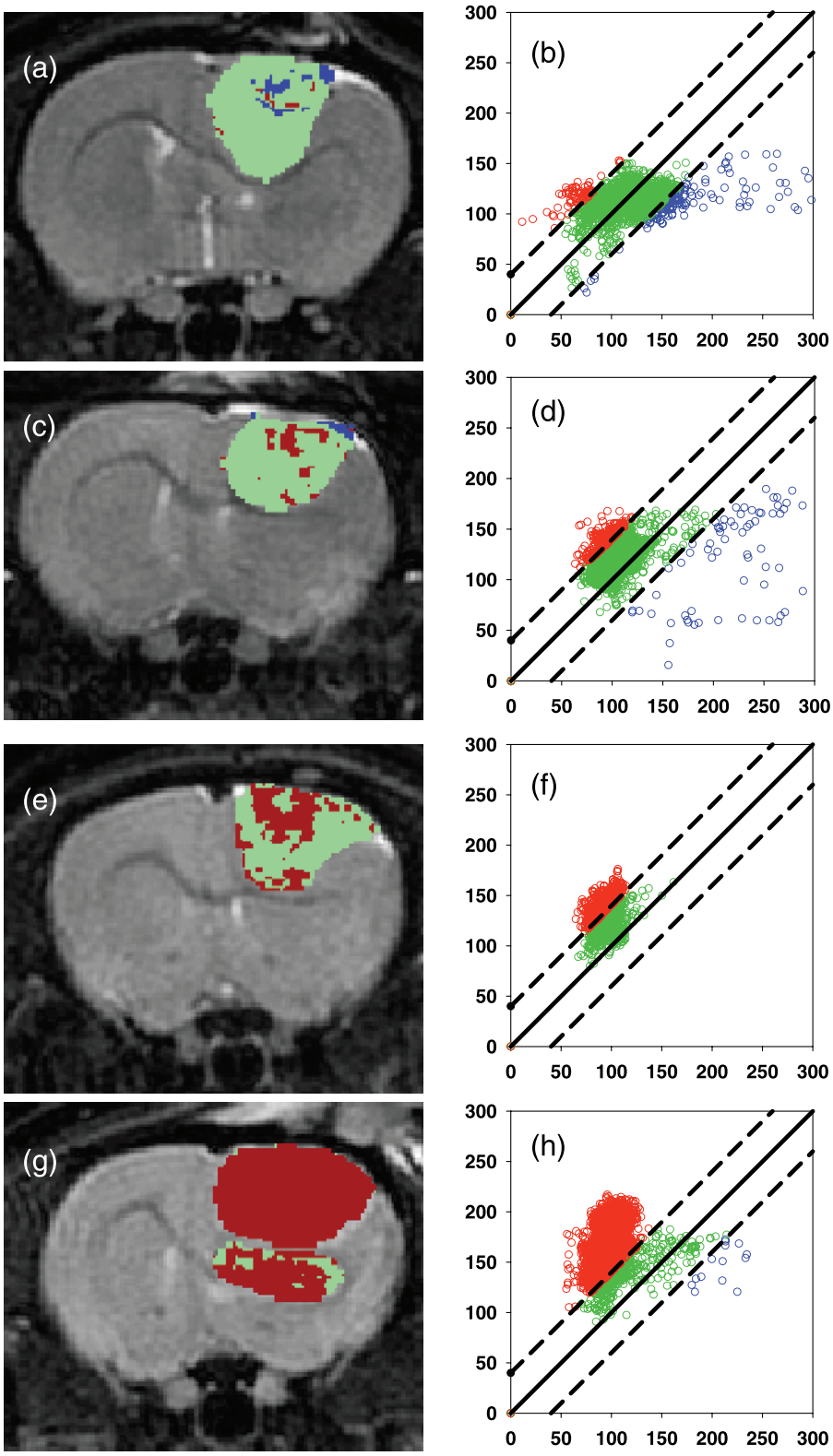

Figure 2. *Representative fDM maps and fDM scatter plots for each treatment group. The animals were treated with: (a and b) 0 mg/kg (control); (c and d) 6.65 mg/kg BCNU; (e and f) 13.3 mg/kg BCNU; (g and h) 26.6 mg/kg BCNU. Images of fDMs (a, c, e, and g) reveal red voxels, which are regions with significant increases in ADC, and blue voxels, which are regions within the tumor with significantly decreased ADC values. The green voxels are tumor regions wherein the ADC values did not change (over the defined threshold level of* $\pm 0.4 \times 10^{-9}$ m^2*/sec) over 4 days following treatment. Scatter plots corresponding to the fDM are voxel ADC values posttreatment (y-axis) as a function of the baseline (time 0) ADC value (x-axis).*

demonstrates how these tumors contained mostly region 3 voxels over this time frame, with the detected changes of V_R and V_B representing only 2.9% and 5.7% of the total tumor volume, respectively. However, the 6.65-mg/kg tumor shown in Figure 2, *c* and *d*, contained responding voxels of V_R = 7.7% and V_B = 2.6%, respectively. The mean V_R (10.6 ± 2.8%) and the mean ADC change (10.7 ± 2.2) for this group were statistically significantly higher ($P < .05$) than those for the control animals (V_R = 3.9 ± 1.7; ΔADC = −0.8 ± 2.7%). For animals treated with 13.3 mg/kg BCNU, as shown on the fDM image (Figure 2*e*) and scatter plots (Figure 2*f*), the responding region V_R (30%) was greater than for both the control and the 6.65-mg/kg–treated animals. The mean V_R (28.7 ± 8.0) and ΔADC (22.9 ± 5.3%) were both statistically greater ($P < .05$) than the values for the 6.65-mg/kg–treated group. In the case of the 26.6-mg/kg BCNU–treated group (Figure 2, *g* and *h*), most of the voxels contained within the tumor mass had increased diffusion values above the threshold (V_R = 90.6%), with only 0.3% V_B voxels. The group mean V_R (62.0 ± 9.0%) and the mean ADC change (49.0 ± 9.7%) were both statistically greater ($P < .05$) than those for the 13.3-mg/kg–treated group.

Traditional measures of brain tumor treatment efficacy were also evaluated in this study. Figure 3*a* shows a survival plot for all groups of animals, revealing that there was a dose-dependent increase in animal survival relative to the control group. Using a log rank test, all groups had a statistically significant difference in median survival posttherapy ($P < .05$). In addition, normalized tumor volume at 4 days posttreatment displayed a decreasing trend with increasing dose of BCNU (Figure 3*b*). Although the groups were not all statistically different, the results of a linear least squares fit showed that the slope was statistically significant ($P < .05$). Lastly, log cell kill (Figure 3*c*) showed an increasing statistical trend ($P < .05$) with dose, although the 6.65-mg/kg group (−0.25 ± 0.08) was not statistically greater ($P > .05$) than the control group (−0.09 ± 0.04). The log cell kill values of the 13.3-mg/kg (1.28 ± 0.18) and the 26.6-mg/kg (3.22 ± 0.51) groups were both statistically different ($P < .001$) from each other and from the control group.

The dose dependence of fDM based on the group means (±SEM) for V_R and V_B values was also calculated. Figure 4 is a plot of V_R and V_B as a function of drug dose (mg/kg). The resulting "best-fit" gradient (2.30 ± 0.40 kg/mg) revealed that V_R was linearly correlated extremely well ($P = 5.8 \times 10^{-6}$) with BCNU dose. In contrast, V_B revealed very little correlation ($P = .87$) with drug dose. Based on these results, it was apparent that, for treatment of the 9L tumor with BCNU, the fDM parameter that was most sensitive to drug-induced cellular changes was V_R. This parameter was then used for the statistical evaluation of fDM with additional outcome measures.

The ability of fDM to predict subsequent therapeutic outcome, as quantified by overall animal survival, was evaluated. Figure 5 displays a plot of percent fDM change (using the parameter V_R) *versus* mean animal survival (days posttreatment). The resulting gradient (1.55 ± 0.44, $P = .002$)

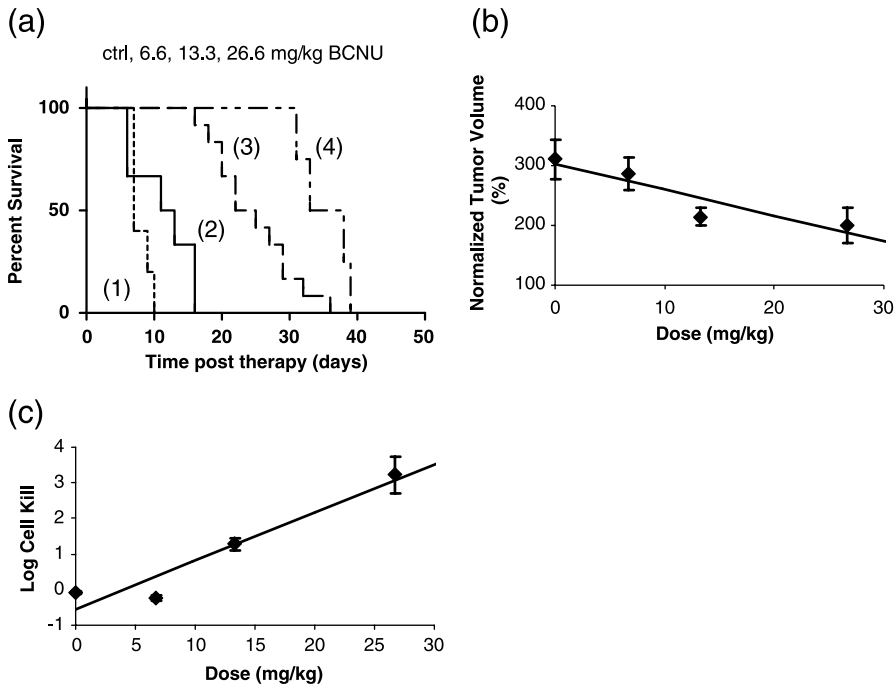

Figure 3. *Dose dependence of traditional therapeutic efficacy measures. (a) Kaplan-Meier animal survival plots of animals treated with: (1) 0 mg/kg, (2) 6.65 mg/kg, (3) 13.3 mg/kg, and (4) 26.6 mg/kg BCNU. The median survival for these groups was 7, 13, 23.5, and 35.5 days posttherapy, respectively. All groups were significantly different, as determined by log rank test (P < .05). (b) Normalized tumor volume at the time fDM analysis was performed (4 days) posttreatment with BCNU as a function of dose. The gradient of the least squares fit was −4.0 ± 1.3 (P = .004), and the intercept was 290 ± 20 (P = 1.4 × 10^{-14}). (c) Log cell kill of the 9L tumor cells as a function of BCNU dose. The gradient of the least squares fit was 0.013 ± 0.02 (P = 3.7 × 10^{-9}), and the intercept was −0.53 ± 0.21 (P = .02). The error bars represent the standard error of the mean for each group.*

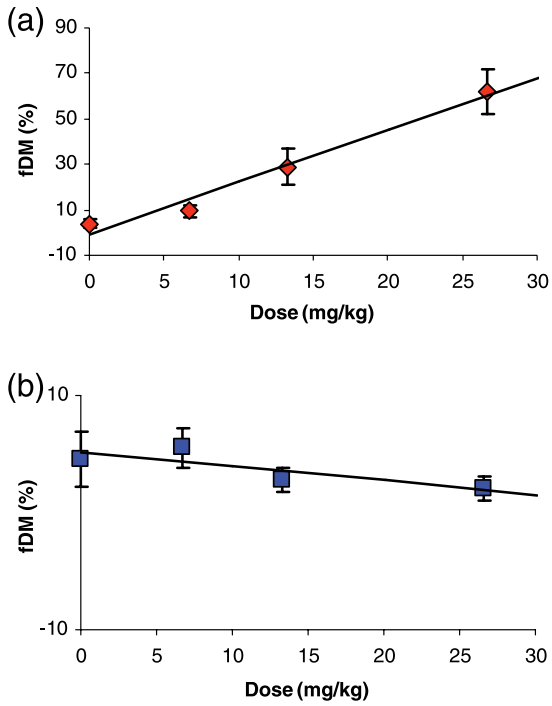

Figure 4. *Dose dependence of detectable changes in fDM parameters V_R and V_B. (a) Mean normalized volume V_R (%) as a function of BCNU dose. The gradient of the least squares fit was 2.30 ± 0.40 ($P = 5.8 \times 10^{-6}$), and the intercept was −1.1 ± 6.2 (P = .87). (b) Mean normalized volume V_B as a function of BCNU dose. The gradient of the least squares fit was −0.10 ± 0.07 (P = .17), and the intercept was 4.5 ± 1.1 (P = .005). The error bars represent the standard error of the mean for each group.*

showed that V_R correlated very well with overall animal survival. This finding strongly supports the use of fDM as a biomarker that is capable of predicting early the overall outcome (survival) following treatment administration.

The fDM approach provides interesting spatial information not provided for in the mean change in ADC approach. We investigated the underlying histologic basis for the observed changes in the detected V_R and V_B fDM regions. Figure 6*a* displays an fDM color overlay on its corresponding anatomic image, which was acquired following treatment with 6.67 mg/kg BCNU. Histologic evaluation of the tumor section prepared from this image region was undertaken. A magnified view of the histologic section of the low-diffusion (V_B) region (high restriction of water mobility) is shown (Figure 6*b*). This region was found to have very high cellular density. In fact, this region contained 153 active mitoses as counted from 10 high-power fields (original magnification, ×40 objective lens). This is reflective of a region with a very high rate of cellular proliferation. In distinct contrast, the region identified by fDM as having very low restricted water diffusion (V_R) was identified by histology to have moderate cellular density. This region was found to have a lower level of cellular proliferation (96 mitoses in 10 high-power fields) than the V_B region (Figure 6*c*).

Discussion

Biomarkers that are sensitive to treatment-induced changes are actively being sought to confirm drug activity or to preselect those patients who are more likely to respond to treatment. An imaging biomarker for this should be capable of detecting relevant drug-induced changes within a tumor. The successful identification and validation of an imaging biomarker that could provide early prediction of treatment outcome would potentially revolutionize cancer drug development and the clinical management of oncology patients. Furthering the urgency of this need is the fact that, after 20 years of research, the clinical benefits of drugs designed to exploit cancer gene-based targets display a significant impact. However, targeted therapies cannot be optimally developed using approaches designed for more traditional cytotoxic chemotherapies, as the maximum tolerated dose may not indicate optimal dose; dose-limiting toxicity may not be proliferation-linked, and myelosuppression side effects cannot be used as surrogate markers of cytotoxicity because many of these effects do not deplete blood cells. These facts highlight the urgent need to find and develop pharmacodynamic and prognostic markers to establish optimal dosing and to confirm that new agents have their desired biochemical effects. An imaging biomarker revealing that cell death occurs in a solid tumor, for example, can demonstrate that an experimental agent kills tumor cells without the long delay traditionally required to reach a clinical endpoint.

Nonimaging-based biomarkers are used by two methods. The first approach uses prognostic markers that are preferably identified through DNA microarrays that match new classes of drugs with the molecular profile of an individual tumor. If a drug is targeted specifically against cells that have a particular mutation, translocation, or gene overexpression, then testing tumor tissues to determine whether

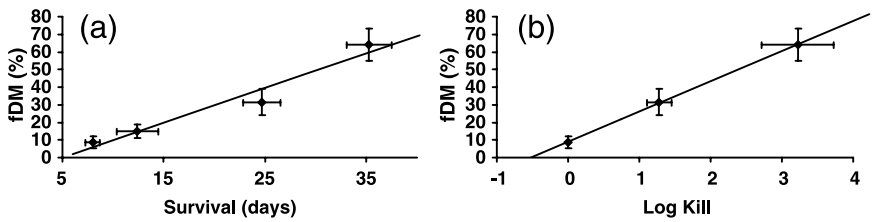

Figure 5. *Correlation of fDM V_R changes with animal survival and cell kill. (a) V_R volumes calculated 4 days post-BCNU therapy are plotted as a function of the median survival for each of the treatment groups. The error bars represent the standard error of the mean for each group. The gradient of the least squares fit was 1.55 ± 0.44 (P = .002), and the intercept was −6.2 ± 9.8 (P = .53). (b) Change in percent fDM versus log cell kill measured using MRI tumor volume measurements over time.*

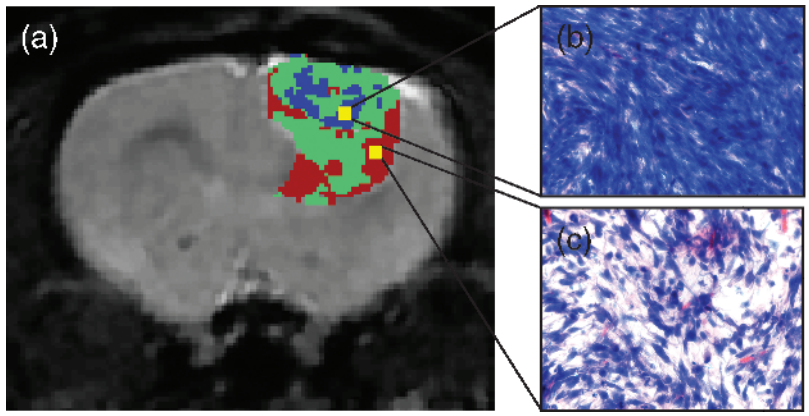

Figure 6. *Histologic evaluation of fDM V_R and V_B regions. (a) A representative fDM image of a 9L tumor showing a heterogeneous response to BCNU (6.65 mg/kg) treatment. The fDM image revealed regions of high (blue) and low (red) restriction of diffusion. (b) H&E-stained slice from a region identified as an fDM (V_B) region of restricted diffusion. This region of high tumor diffusional restriction contained decreased amounts of extracellular space, as shown in the H&E image. In addition, this region was found to contain 153 mitoses in 10 high-power fields (original magnification, ×40 objective lens), reflecting a high rate of proliferation. (c) A region of low restriction (V_R) is shown to have a moderate level of cellular density, as shown in the H&E image. This region contained 96 mitoses in 10 high-power fields, reflecting mitoses that are fewer than those in the previous region (V_B).*

such molecular profile is present in a tumor may help clinicians avoid prescribing ineffective treatments. The second method uses pharmacodynamic markers that are designed to provide information as to whether a drug is manifesting its intended biochemical effect, and, if so, to what extent. In the long term, these pharmacodynamic effects could be used as surrogate markers for clinical response. However, these nonimaging-based approaches use tissue specimens and, as such, do not take into account the tremendous heterogeneity exhibited by tumors. Moreover, different agents will target different molecular sites within the tumor, thus potentially requiring a plethora of biomarkers, with each requiring independent validation.

A noninvasive imaging approach is preferred because imaging is sensitive and minimally invasive, and can provide multidimensional multislice images with exquisite resolution at multiple time points. Initial diffusion MRI Clinical Studies have revealed that treatment-induced changes could be observed within tumors [11,33–37]. The functional diffusion mapping approach evaluated in this study is an *in vivo*, translatable, quantifiable, noninvasive multislice imaging biomarker, which was shown to be very sensitive to early therapy-induced alterations in tumor cell membrane integrity [28,29]. Thus, the use of changes in tumor water diffusion as biomarker for microscopic changes associated with successful treatment intervention provides an important opportunity for assessing a broad range of drugs.

An important aspect of translating any biomarker is that it undergoes adequate validation and should correlate with biologically relevant endpoints. In this current study, the dose response of fDM in brain tumors was compared to traditional endpoints, including tumor growth, cell kill, histopathology, and animal survival. Compared to tumor volume and cell kill measures of outcomes that had significant trends but no statistical differences between vehicle control and 6.65-mg/kg–treated animals, fDM was shown to be a superior measurement of treatment efficacy (Figure 3, *b* and *c*).

An excellent correlation of fDM response with increasing BCNU dose (Figure 4*a*) and the significant differences in fDM-measured responses between all dosage groups were shown. The "gold standard" of efficacy measures in orthotopic experimental tumor models has traditionally been animal survival. In this current study, we found fDM response quantified at 4 days posttreatment to be highly correlated with animal survival and cell kill (Figure 5, *a* and *b*). Perhaps one of the most interesting findings was that the low dose (6.65 mg/kg) was barely effective as it only increased survival by an average of 5.5 days; however, fDM was, in fact, sensitive enough to detect a significant difference from the control group of animals and from higher treatment doses. Thus, the excellent correlation of fDM change with animal survival outcome provides compelling evidence that this is a valid biomarker for the early detection and prediction of biologically relevant outcome measures (survival and cell kill). Furthermore, fDM was recently shown to be able to stratify therapeutically responsive glioma patients from nonresponsive patients in as early as 3 weeks into a 6-week to a 7-week treatment schedule [29]. These data revealed that fDM could identify early patients who are prone to having significantly poorer survival and time-to-progression from those patients who would have a much more responsive outcome [29]. These data, along with clinical results, reveal that fDM can be effectively used as a predictive biomarker for the early stratification of tumor response before completion of therapy in both preclinical and clinical oncology studies.

An important aspect of fDM is that it maintains spatial imaging information, thus providing it with an exciting advantage over other possible biomarker approaches, such as genomic and proteomic approaches. This is a particular advantage given that treatment response can be extremely heterogeneous due to a variety of reasons, such as differential drug delivery and spatially varying heterogeneity in tumor phenotype expression levels. The advantage of this is quite evident as revealed in this histologic assessment (Figure 6) of

different fDM regions (V_R and V_B). These data revealed that V_R correlated with a region of significant treatment-induced cell death. However, foci of tumor regions undergoing rapid cellular proliferation were also detected by V_B as regions of greatly reduced water mobility, confirmed by histology as focal regions of high cell density along with high mitotic index. These regions of increased proliferation were not observed with higher doses of BCNU treatment (Figure 2, *e*–*h*). In fact, the increased dose had an additional effect of increasing the overall percentage of the V_R region and of shifting the distribution of green voxels to a higher level (on average), as shown on scatter plots (Figure 2, *f* and *h*). This indicates that a dynamic shift in the overall tumor cytoarchitecture toward a loss of cell density/membrane integrity occurred following treatment.

In this study, it has been shown that fDM is a viable, quantifiable, and early imaging biomarker of treatment response, as it was shown to correlate with traditional biomarkers of efficacy such as survival and cell kill. The advantages of fDM include the following: 1) acquisition of this imaging data can be accomplished rapidly (in seconds); and 2) it provides a much more timely readout over traditional outcome measures. The ability to rapidly assess efficacy following treatment initiation provides an important opportunity to more rapidly evaluate drug dosages and combinations in preclinical studies. Moreover, because fDM is a translatable technique, inclusion of fDM in phase 1 and 2 clinical trials would provide a sensitive means to detect treatment efficacy, which is especially valuable in dose escalation protocols. Furthermore, fDM provides the potential to truly individualize patient treatment regimens through unbiased quantization of early treatment response. This has tremendous clinical significance as it could facilitate early identification of patients who are nonresponsive to a specific intervention and thereby provide more time to try alternative therapies. Utilization of fDM in this fashion would be an invaluable and cost-effective approach for managing individual patients undergoing anticancer treatment. Further impact could be seen in improvements in patients' quality of life and extension of overall survival.

In conclusion, this study has validated fDM as an imaging biomarker in a preclinical tumor model. Although this approach should be further examined in additional tumor models, we have shown clearly the power of using fDM as a biomarker for the early detection of cancer treatment response in the 9L model. The important properties of this *in vivo* imaging biomarker include the following: its translatability to the clinical setting [28,29]; its quantitative nature, which is independent of the manufacturing of the MRI instrument and of magnetic field strength; the close correlation with primary biologic endpoints, including overall histology, cell kill, and survival; and its ease of use and cost-effectiveness. These results provide an important foundation for using diffusion MRI to individualize the treatment of cancer patients. Data presented in this study provide compelling evidence for the need to rapidly advance the application of diffusion MRI and fDM in the preclinical setting and in the oncology clinic.

References

[1] Le Bihan D, Breton E, Lallemand D, Grenier P, Cabanis E, and Laval-Jeantet M (1986). MR imaging of intravoxel incoherent motions: application to diffusion and perfusion in neurologic disorders. *Radiology* **161,** 401–407.

[2] Ross BD, Chenevert TL, Kim B, and Ben-Joseph O (1994). Magnetic resonance imaging and spectroscopy: application to experimental neurooncology. *J Magn Reson Biol Med* **1,** 89–106.

[3] Zhao M, Pipe JG, Bonnett J, and Evelhoch JL (1996). Early detection of treatment response by diffusion-weighted ^{1}H-NMR spectroscopy in a murine tumour *in vivo*. *Br J Cancer* **73,** 61–64.

[4] Chenevert TL, McKeever PE, and Ross BD (1997). Monitoring early response of experimental brain tumors to therapy using diffusion magnetic resonance imaging. *Clin Cancer Res* **3,** 1457–1466.

[5] Ross BD, Stegman LD, Chenevert TL, and Rehemtulla A (1999). The role of magnetic resonance in the evaluation of cancer therapeutics. *Clin Cancer Res* **5,** 3870s–3871s.

[6] Galons JP, Altbach MI, Paine-Murrieta GD, Taylor CW, and Gillies RJ (1999). Early increases in breast tumor xenograft water mobility in response to paclitaxel therapy detected by non-invasive diffusion magnetic resonance imaging. *Neoplasia* **1,** 113–117.

[7] Lyng H, Haraldseth O, and Rofstad EK (2000). Measurement of cell density and necrotic fraction in human melanoma xenografts by diffusion weighted magnetic resonance imaging. *Magn Reson Med* **43,** 828–836.

[8] Chinnaiyan AM, Prasad U, Shankar S, Hamstra DA, Shanaiah M, Chenevert TL, Ross BD, and Rehemtulla A (2000). Combined effect of tumor necrosis factor–related apoptosis-inducing ligand and ionizing radiation in breast cancer therapy. *Proc Natl Acad Sci USA* **97,** 1754–1759.

[9] Evelhoch JL, Gillies RJ, Karczmar GS, Koutcher JA, Maxwell RJ, Nalcioglu O, Raghunand N, Ronen SM, Ross BD, and Swartz HM (2000). Applications of magnetic resonance in models systems: cancer therapeutics. *Neoplasia* **2,** 152–165.

[10] Stegman LD, Rehemtulla A, Hamstra D, Rice D, Jonas SJ, Stout KL, Chenevert TL, and Ross BD (2000). Diffusion MRI detects early events in the response of a glioma model to the yeast cytosine deaminase gene therapy strategy. *Gene Ther* **7,** 1005–1010.

[11] Chenevert TL, Stegman LD, Robertson PL, Greenberg HS, Rehemtulla A, and Ross BD (2000). Diffusion magnetic resonance imaging: an early surrogate marker of therapeutic efficacy in brain tumors. *J Natl Cancer Inst* **92,** 2029–2036.

[12] Ross BD, Chenevert TL, and Rehemtulla A (2002). Magnetic resonance imaging in cancer research. *Eur J Cancer* **38,** 2147–2156.

[13] Rehemtulla A, Hall DE, Stegman LD, Presad U, Chen G, Bhojani MS, Chenevert TL, and Ross BD (2002). Molecular imaging of gene expression and efficacy following adenoviral-mediated brain tumor gene therapy. *Mol Imaging* **1,** 43–55.

[14] Chenevert TL, Meyer CR, Moffat BA, Rehemtulla A, Mukherji SK, Gebarski SS, Quint DJ, Robertson PL, Lawrence TS, Junck LR, et al. (2002). Diffusion MRI: a new strategy for assessment of cancer therapeutic efficacy. *Mol Imaging* **1,** 336–343.

[15] Jennings D, Hatton BN, Guo J, Galons JP, Trouard TP, Raghunand N, Marshall J, and Gillies RJ (2002). Early response of prostate carcinoma xenografts to docitaxel chemotherapy monitored with diffusion MRI. *Neoplasia* **4,** 255–262.

[16] Ross BD, Lawrence TS, Mukherji SK, Gebarski SS, Quint DJ, Johnson TD, Junck LR, Robertson PL, Muraszko KM, Dong Q, et al. (2003). Evaluation of cancer therapy using diffusion magnetic resonance imaging. *Mol Cancer Ther* **2,** 581–587.

[17] Moffat BA, Chenevert TL, and Ross BD (2004). Diffusion MR imaging in adult neoplasia. In J Gillard, A Waldman, P Barker (Eds.), Physiological MR in Clinical Neuroscience. CUP, Cambridge.

[18] Hall DE, Moffat BA, Stojanovska J, Johnson TD, Li Z, Hamstra DA, Rehemtulla A, Chenevert TL, Carter J, Pietronigro D, et al. (2004). Therapeutic efficacy of DTI-015 using diffusion magnetic resonance imaging as an early surrogate marker. *Clin Cancer Res* **10,** 7852–7859.

[19] Hamstra DA, Lee KC, Tychewicz JM, Schepkin VD, Moffat BA, Chen M, Dornfeld KJ, Lawrence TS, Chenevert TL, Ross BD, et al. (2004). The use of ^{19}F spectroscopy and diffusion-weighted MRI to evaluate differences in gene-dependent enzyme prodrug therapies. *Mol Ther* **10,** 916–928.

[20] Moffat BA, Hall DE, McConville PJ, Stojanovska J, Chenevert TL, Rehemtulla A, and Ross BD (2004). Diffusion imaging for evaluation of tumor therapies in pre-clinical animal models. *Magma* **17,** 249–259.

[21] Rodrigues LM, Stubbs M, Robinson SP, Newell B, Mansi J, and Griffiths

JR (2004). The C-neu mammary carcinoma in Oncomice; characterization and monitoring response to treatment with herceptin by magnetic resonance methods. *Magma* **17,** 260–270.

[22] Schepkin VD, Ross BD, Chenevert TL, Rehemtulla A, Sharma S, Kumar M, and Stojanovska J (2005). Sodium MRI of chemotherapeutic response in a rat glioma. *Magn Reson Med* **53,** 85–92.

[23] Lee KC, Hamstra DA, Bullarayasamudram S, Bhojani MS, Moffat BA, Dornfeld KJ, Ross BD, and Rehemtulla A (2006). Fusion of the HSV-1 tegument protein vp22 to cytosine deaminase confers enhanced bystander effect and increased therapeutic benefit. *Gene Ther* **13,** 127–137.

[24] Schepkin VD, Chenevert TL, Kuszpit K, Lee KC, Meyer CR, Johnson TD, Rehemtulla A, and Ross BD (2006). Sodium and proton diffusion MRI as biomarkers for early therapeutic response in subcutaneous tumors. *Magn Res Imaging* (in press).

[25] Lee KC, Hall DE, Hoff BA, Moffat BA, Sharma S, Chenevert TL, Meyer CR, Leopold WR, Johnson TD, Rehemtulla A, et al. (2006). Dynamic imaging of emerging resistance during cancer therapy. *Cancer Res* (in press).

[26] Jordan BF, Runquist M, Raghunand N, Baker A, Williams R, Kirkpatrick L, Powis G, and Gillies RJ (2005). Dynamic contrast-enhanced and diffusion MRI show rapid and dramatic changes in tumor microenvironment in response to inhibition of HIF-1alpha using PX-478. *Neoplasia* **7,** 475–485.

[27] Roth Y, Tichler T, Kostenich G, Ruiz-Cabello J, Maier SE, Cohen JS, Orenstein A, and Mardor Y (2004). High-*b*-value diffusion-weighted MR imaging for pretreatment prediction and early monitoring of tumor response to therapy in mice. *Radiology* **232,** 685–692.

[28] Moffat BA, Chenevert TL, Lawrence TS, Meyer CR, Johnson TD, Dong Q, Tsien C, Mukherji S, Quint DJ, Gebarski SS, et al. (2005). Functional Diffusion Map (fDM): a noninvasive MRI biomarker for early stratification of clinical brain tumor response. *Proc Natl Acad Sci USA* **102,** 5524–5529.

[29] Hamstra DA, Chenevert TL, Moffat BA, Johnson TD, Meyer CR, Mukherji SK, Quint DJ, Gerbarski SS, Fan X, Tsien C, et al. (2005). Evaluation of the functional diffusion map as an early biomarker of time-to-progression and overall survival in high grade glioma. *Proc Natl Acad Sci USA* **102,** 16759–16764.

[30] Meyer CR, Boes JL, Kim B, and Bland PH (1997). Demonstration of accuracy and clinical versatility of mutual information for automatic multimodality image fusion using affine and thin-plate spline warped geometric deformations. *Med Image Anal* **1,** 195–206.

[31] Ross BD, Zhao Y-J, Neal ER, Stegman LD, Ercolani M, Ben-Yoseph O, and Chenevert TL (1998). Contributions of cell kill and posttreatment tumor growth rates to the repopulation of intracellular 9L tumors after chemotherapy: an MRI study. *Proc Natl Acad Sci USA* **95,** 7012–7017.

[32] Sugahara T, Korogi Y, Kochi M, Ikushima I, Shigematu Y, Hirai T, Okuda T, Liang L, Ge Y, Komohara Y, et al. (1999). Usefulness of diffusion-weighted MRI with echo-planar technique in the evaluation of cellularity in gliomas. *J Magn Reson Imaging* **9,** 53–60.

[33] Mardor Y, Pfeffer R, Spiegelmann R, Roth Y, Maier SE, Nissim O, Berger R, Glicksman A, Baram J, Orenstein A, et al. (2003). Early detection of responses to radiation therapy in patients with brain malignancies using conventional and high *b*-value diffusion-weighted magnetic resonance imaging. *J Clin Oncol* **21,** 1094–1100.

[34] Kremser C, Judmaier W, Hein P, Griebel J, Lukas P, and de Vries A (2003). Preliminary results on the influence of chemoradiation on apparent diffusion coefficients of primary rectal carcinoma measured by magnetic resonance imaging. *Strahlenther Onkol* **179,** 641–649.

[35] Hein PA, Kremser C, Judmaier W, Griebel J, Pfeiffer KP, Kreczy A, Hug EB, Lukas P, and DeVries AF (2003). Diffusion-weighted magnetic resonance imaging for monitoring diffusion changes in rectal carcinoma during combined, preoperative chemoradiation: preliminary results of a prospective study. *Eur J Radiol* **45,** 214–222.

[36] Theilmann RJ, Borders R, Trouard TP, Xia G, Outwater E, Ranger-Moore J, Gillies RJ, and Stopeck A (2004). Changes in water mobility measured by diffusion MRI predicts response of metastatic breast cancer to chemotherapy. *Neoplasia* **6,** 831–837.

[37] Mardor Y, Roth Y, Ochershvilli A, Spiegelmann R, Tichler T, Daniels D, Maier SE, Nissim O, Ram Z, Baram J, et al. (2004). Pretreatment prediction of brain tumors' response to radiation therapy using high *b*-value diffusion-weighted MRI. *Neoplasia* **6,** 136–142.